Int. J. Electrochem. Sci., 17 **(2022)** Article Number: 22121, doi: 10.20964/2022.12.06

International Journal of
ELECTROCHEMICAL
SCIENCE
www.electrochemsci.org

Effect of Different g-C_3N_4 Content on Properties of $NiCo_2S_4$/g-C_3N_4 Composite as Electrode Material for Supercapacitor

Meijie Ding[1], *Zhiqiang Wei*[2,*] , *Xiaojun Zhu*[3], *Dexue Liu*[1,*]

[1] State Key Laboratory of Advanced Processing and Recycling of Non-ferrous Metals, and School of Material and Engineering, Lanzhou University of technology, Lanzhou 730050, China
[2] State Key Laboratory of Advanced Processing and Recycling of Non-ferrous Metals, and School of Science, Lanzhou University of Technology, Lanzhou, 730050, China
[3] Jinchuan Group CO., LTD. National Nickel and Cobalt Advanced Materials Engineering Research Center, Lanzhou 730050, China
[*]E-mail: qianweizuo@163.com, dxliu@lut.edu.cn

Received: 9 April 2022 / *Accepted:* 13 August 2022 / *Published:* 17 November 2022

Electronic conductivity of pure $NiCo_2S_4$ is limited, and fortunately, g-C_3N_4 has been explored in recent years for electrochemical applications with considerable potential. $NiCo_2S_4$/g-C_3N_4 nanocomposites, improving greatly the cycle life of supercapacitors, are synthesized via simple one-step hydrothermal method for supercapacitor electrode materials in this paper. The composite of g-C_3N_4 and $NiCo_2S_4$ materials can provide a good bridge for ion transport in the electrochemical reaction process, and can also provide more active sites for the electrochemical reaction due to g-C_3N_4 two-dimensional lamellar structure having a large specific surface area. It is demonstrated that $NiCo_2S_4$/g-C_3N_4 electrodes can achieve specific capacitance of 1229.9 F/g under a current density of 5 A/g and cycling life of 2000 cycles by retaining 66.24% of the energy storage capability in the paper. In general, the potential of g-C_3N_4 in electrochemical applications can be expanded by changing the molar composition of g-C_3N_4.

Keywords: $NiCo_2S_4$; electrochemical; supercapacitor; hydrothermal method

1. INTRODUCTION

With the development of science and technology and the progress of human society, the serious environmental pollution caused by traditional fossil energy (such as coal, oil, natural gas, etc.) has seriously threatened people's health [1-5]. Therefore, the development and utilization of green and pollution-free energy storage devices has become the main way to solve the energy problem [6-9]. The emergence of supercapacitors and lithium ion batteries has greatly solved the described problem above, and however, the low power density of lithium-ion secondary batteries and the low energy density of traditional capacitors can hardly meet the needs of electric vehicles, space shuttles and other fields [10-

13]. It is worth noting that the advantages of supercapacitors, such as excellence power density, large capacity, rapid charge and discharge, and the clean and environmental protection have become the focus of current research [14-16]. Supercapacitors (SCs) is also called electrochemical capacitors. Generally, SCs can be classified into two types: electrical double-layer capacitors (EDLCs) and Faradic redox reaction pseudocapacitors [17-19]. Among the two types, pseudocapacitors, usually including conductive polymers and metal oxides, can provide much higher specific capacitance and higher energy density than that of double-layer capacitors and attract widespread attention from researchers [20-22]. SCs have been known as one of the most promising candidates for high-power applications owing to their attractive properties, including high power density, long cycle life and fast charge/discharge rate [23-24]. In the circumstance, electrode materials, deemed as an alternative for finite fossil fuels, have caused significant interest in recent years due to their high chemical redox reactivity, inexpensive and environmentally benign and good electrode materials can greatly improve the electrochemical performance of electrode materials [25-26]. Among many electrode materials, transition metal compounds have become one of the candidates for supercapacitor electrode materials due to their excellent electrochemical stability, wide potential range, good cycling stability, high reversibility, high conductivity and high specific capacitance [27-29].

Compared with the remarkable electrochemical properties of $NiCo_2O_4$, spinel $NiCo_2S_4$ is explored for its more striking electrochemical performance, which has become a new hot topic [30]. However, $NiCo_2S_4$ still has the defects of low conductivity and material volume change during charge-discharge processes, which seriously hindered their practical applications. Therefore, $NiCo_2S_4$ of various morphologies (such as nanotubes, nanoplates, hollow spheres and so on) was prepared to improve its electrochemical properties. Han et al.[31] using the carbon spheres as the sacrificial template, successfully synthesized $NiCo_2S_4/Co_9S_8$ hollow spheres through the solvothermal method and anion exchange process. Through testing and research, the capacitance retention rate is up to 85% after 10000 cycles.

2. EXPERIMENTAL

2.1 Synthesis of $NiCo_2S_4$/g-C_3N_4 nanomaterials

$NiCo_2S_4$/g-C_3N_4 nanomaterials were prepared by a hydrothermal method. In a typical composition. Firstly, four portions of 3 mmol $Ni(NO)_2{\cdot}6H_2O$ and 6 mmol $Co(NO)_2{\cdot}6H_2O$ were poured into four beakers of 80 ml deionized water with magnetic stirring until homogeneous solution, respectively. 0.3 mmol, 0.6 mmol, 0.9 mmol and 1.2 mmol of g-C_3N_4 were weighed according to the molar content ratios of g-C_3N_4 and $NiCo_2S_4$ of 0.1:1, 0.2:1, 0.3:1 and 0.4:1, respectively. Then, the weighed g-C_3N_4 was dissolved into the previously prepared quadruplicate solution. The sample number is marked as $NiCo_2S_4$/g-C_3N_4-1, $NiCo_2S_4$/g-C_3N_4-2, $NiCo_2S_4$/g-C_3N_4-3, $NiCo_2S_4$/g-C_3N_4-4 according to molar ratio (0.1:1, 0.2:1, 0.3:1 and 0.4:1) between g-C_3N_4 and $NiCo_2S_4$. Next, 24 mmol $(NH_2)_2CS$ added into the above four mixed solutions with stirring for continually 30 minutes, respectively.

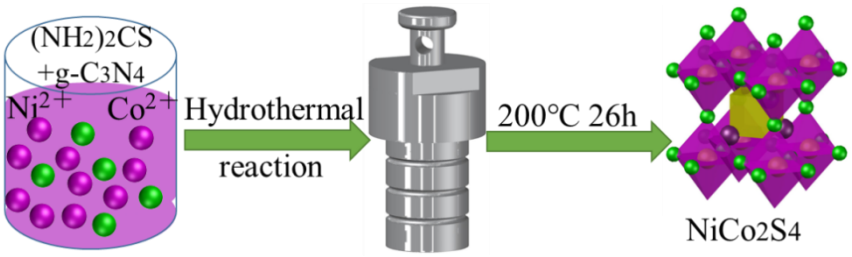

Figure 1. The schematic illustration of the synthesis of different $NiCo_2S_4$/g-C_3N_4 samples by hydrothermal method.

Finally, the mixture was transferred to a vacuum drying oven, which is kept at 200 ℃ for 26 h. After cooling to the room temperature, the synthesized sample were first washed with deionized water, subsequent with ethanol several times via centrifugation before drying overnight for 24 h. Fig.1 shows schematic illustration of the fabrication of different molar ratios $NiCo_2S_4$/g-C_3N_4.

2.2. Characterizations

The morphologies and microstructures were tested using scanning electron microscope (SEM), The crystal structure was characterized by powder X-ray diffraction (XRD) with Bruker D8 Advance using Cu-Kα radiation. X-ray photoelectron spectroscopy (XPS) analyzes the sample by X-rays to obtain the composition of the analyze.

2.3. Electrochemical measurement

Electrochemical properties of electrode materials were measured on electrochemical workstation of a three-electrode system in 4 M KOH aqueous electrolyte. The working electrode was fabricated by mixing electrode slurry, which is made of 80 wt% active material, 10 wt% acetylene black, and 10 wt% polyvinylidene flfluoride (PVDF). The slurry was coated on a piece of Ni foam (1 cm×1 cm), and dried overnight at 80 °C. Cyclic voltammetry (CV) curves were measured by electrochemical workstation from different scan rate in a potential window of 0.0-0.6 V. Galvanostatic charge-discharge (GCD) curves were recorded in a potential window of 0.0-0.5 V. The electrochemical impedance spectroscopies (EIS) spectra were measured in the frequency range of 10^{-2} to 10^{5} Hz.

Electrochemical properties of electrode materials were measured on electrochemical workstation of a three-electrode system in 4 M KOH aqueous electrolyte. The working electrode was fabricated by mixing electrode slurry, which is made of 80 wt% active material, 10 wt% acetylene black, and 10 wt% polyvinylidene fluoride (PVDF). The slurry was coated on a piece of Ni foam (1 cm×1 cm), and dried overnight at 80 °C. Cyclic voltammetry (CV) curves were measured by electrochemical workstation from different scan rates in a potential window of 0.0-0.6 V. Galvanostatic charge-discharge (GCD) curves were recorded in a potential window of 0.0-0.5 V. The electrochemical impedance spectroscopies (EIS) spectra were measured in the frequency range of 10^{-2} to 10^{5} Hz. The specific capacity of the different $NiCo_2S_4$/g-C_3N_4 samples electrode were calculated using the following equations [32-34].

$$C=\frac{I\Delta t}{m} \quad (1)$$

where C is the specific capacitance of anode material. m represents the mass of electroactive materials. I and Δt stand for the discharge current and discharge time, respectively.

3. RESULTS AND DISCUSSION

Considering the two-dimensional lamellar structure and excellent properties of g-C_3N_4 Graphene Quantum Dots (GQDs), we have proposed the design, preparation and testing of $NiCo_2S_4$/g-C_3N_4 nanocomposites. The molar ratios of g-C_3N_4 and $NiCo_2S_4$ is 0.1:1, 0.2:1, 0.3:1 and 0.4:1, respectively. Because the molar content is more convenient to measure the amount of material in the process of material composite. With the increase of g-C_3N_4 composite proportion at different current densities. In the next subsection,we will have a analysis of the material properties.

The X-ray diffffraction (XRD) patterns of $NiCo_2S_4$/g-C_3N_4-1, $NiCo_2S_4$/g-C_3N_4-2, $NiCo_2S_4$/g-C_3N_4-3 and $NiCo_2S_4$/g-C_3N_4-4 are shown in the inset of Fig.2, in which the diffraction peak positions of the four electrode materials are 16.3°, 26.9°, 31.6°, 38.3°, 50.5° and 55.3°, respectively, and they are consistent with the standard card (PDF#20-0782). The result also implies that the corresponding crystal planes are (1 1 1), (2 2 0), (3 1 1), (4 0 0), (5 1 1) and (4 4 0), respectively.

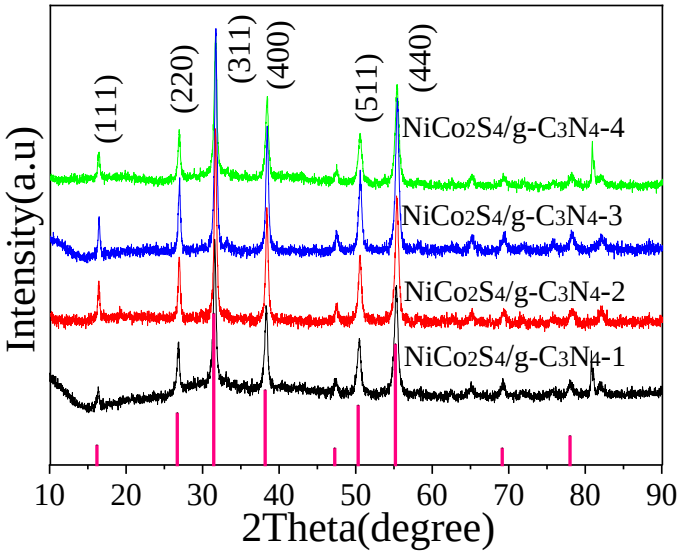

Figure 2. XRD pattern of the different molar ratios $NiCo_2S_4$/g-C_3N_4

The SEM images of the electrode material with different proportions of g-C_3N_4 and $NiCo_2S_4$ composites are shown in Fig.3 (a), (b), (c) and (d), which the corresponding composite molar ratio is 0.1:1, 0.2:1, 0.3:1 and 0.4:1 in the experiment, respectively. It can be seen from the figure that the morphology of the four electrode materials has a porous structure, which can greatly increase the specific surface area of the electrode materials. A large specific surface area can provide more active sites for electrochemical reactions, thus further improving the electrochemical performance of the electrode materials. Further the ingredient of the composition and the valence state information of electrode materials are investigated and evaluated by the X-ray photoelectron spectroscopy (XPS).

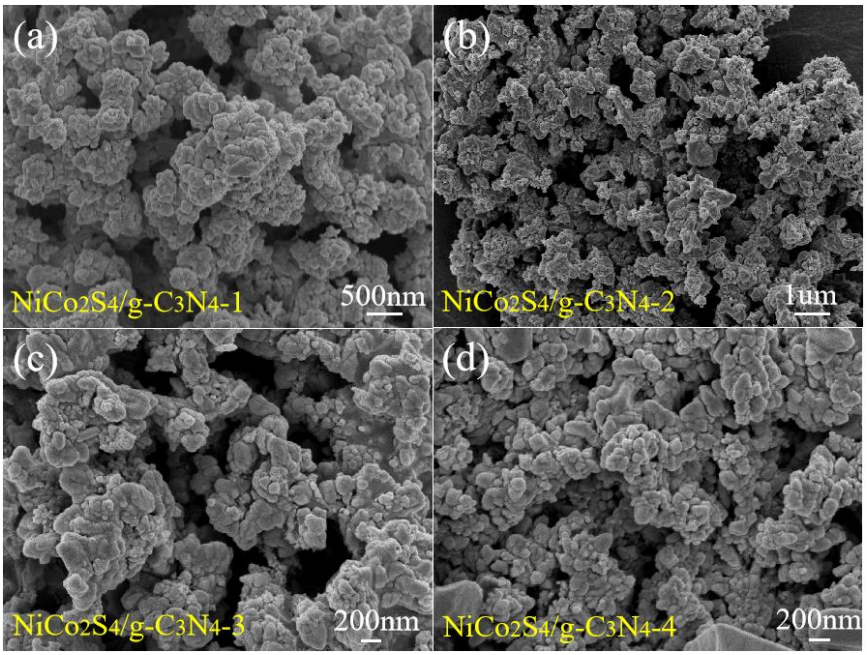

Figure 3. (a-d) SEM images of the different $NiCo_2S_4$/g-C_3N_4 samples

Fig. 4(a-f) shows the high-resolution spectra of the Ni 2p, Co 2p, S 2p, C 1s and N 1s states, respectively. Ni 2p was split into Ni $2p_{3/2}$ and Ni $2p_{1/2}$ with two states. Moreover, each state was further deconvoluted into two sub-states. The high-intensity sub-states of Ni $2p_{3/2}$ at 875.13 eV and 856.6 eV corresponded to the tetrahedrally located Ni^{2+} state, and those of Ni $2p_{1/2}$ at 869.94 eV and 852.65 eV corresponded to the octahedral Ni^{3+} state. Similarly, the Co 2p spectrum was deconvoluted into four peaks, i.e., Co $2p_{3/2}$ (781.4 and 779.8 eV) and Co $2p_{1/2}$ (793.5 and 794.4 eV) with a spin-energy separation of 14.6 eV corresponding to the Co^{3+} and Co^{2+} states of the cobalt within $NiCo_2S_4$ nanoflakes, respectively [35-36]. The small peaks were assigned to the satellite peaks of the Ni 2p and Co 2p states. In Fig.4(d), the peaks at 162.85 eV and 161.71 eV are corresponding to S $2p_{1/2}$ and S $2p_{3/2}$, respectively. The result that peaks are located at 284.8 eV, 286.5 eV and 288.7 eV in Fig.4(e) shows that three carbon contributions, C-C, C-N and O-C=O, are fit by the C 1s spectrum. Then as shown in Fig.4(f), high-resolution N 1s spectrum is composed of three parts, Pyridinic-N, Pyrrolic-N and Ggraphitic-N, and their combination energy are 399.8 eV, 401.3 eV and 402.1 eV, respectively.

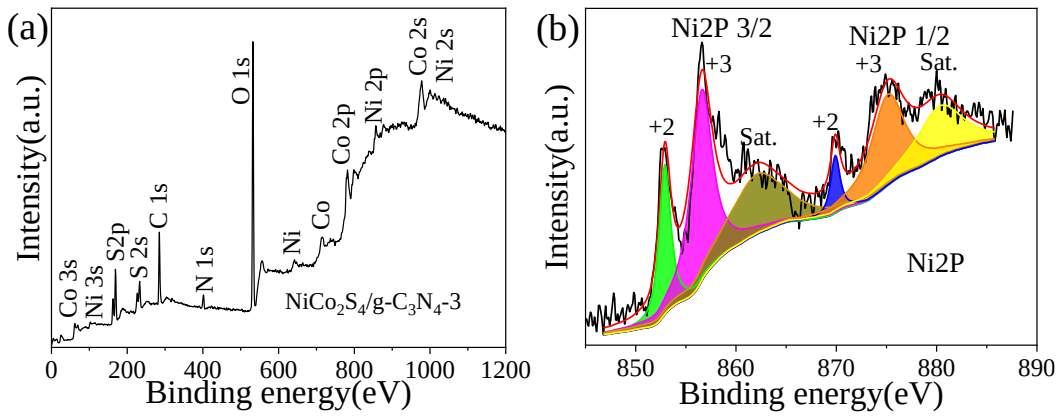

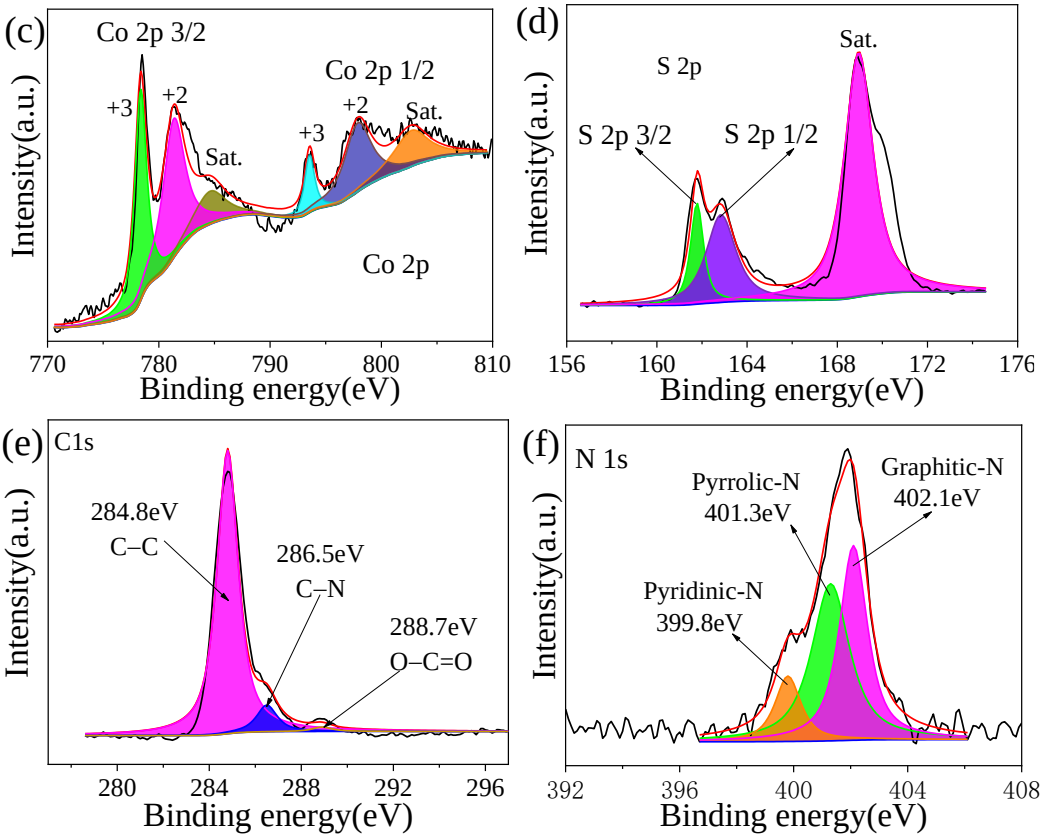

Figure 4. (a) XPS survey spectra of $NiCo_2S_4$/g-C_3N_4-3 electrode; (b–f) high resolution Co 2p, Ni 2p, S 2p, C 1s and N1s spectra for the $NiCo_2S_4$/g-C_3N_4-3.

The microstructure and surface area of the composite are further characterized by isothermal adsorption-desorption curve and pore size distribution, shown in Fig.5(a) and Fig.5(b), where the specific surface areas of $NiCo_2S_4$/g-C_3N_4-1, $NiCo_2S_4$/g-C_3N_4-2, $NiCo_2S_4$/g-C_3N_4-3 and $NiCo_2S_4$/g-C_3N_4-4 electrode materials are 131.3 m^2/g, 111.1 m^2/g, 88.0 m^2/g and 194.9 m^2/g, respectively. It can be seen from Fig.5(a) that the nitrogen adsorption curve and desorption curve almost coincide when the relative pressure P/P_0 of $NiCo_2S_4$/g-C_3N_4 electrode material is less than 0.4, the adsorption capacity also increases with the increase of relative pressure, and the electrode material has micropore of 10-50 nm. Sequentially, Fig.5(b) describes the pore diameter distribution curve of the electrode material, and the number of macropores and mesopores accounts for around 45% and 55% in the pore size distribution diagram, respectively. The average pore size of adsorption is within 20-75 nm. The experiments results illustrate that the electrode materials with a larger specific surface area and a more micropore are beneficial for the penetration of electrolyte, and it provides a more active sites for electrochemical reaction [37-38].

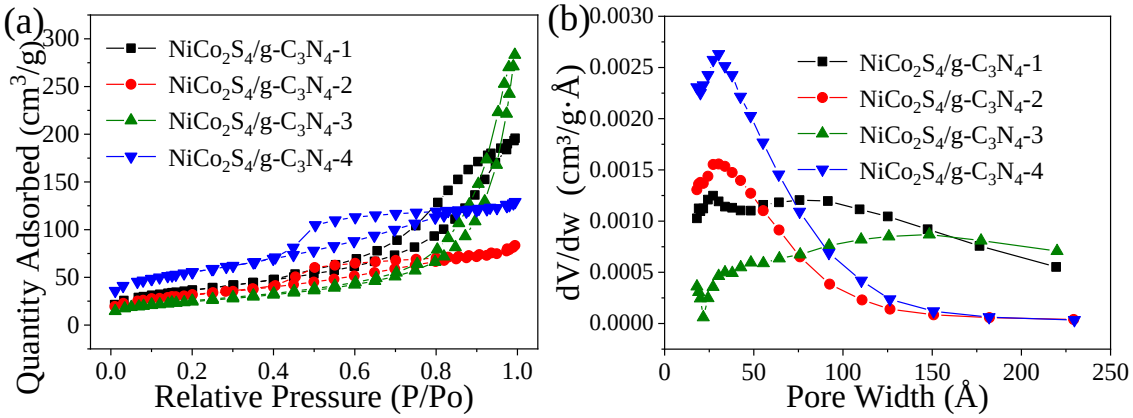

Figure 5. (a) Nitrogen adsorption-desorption isotherms of the different molar ratios $NiCo_2S_4$/g-C_3N_4; (b) the pore size distribution curve.

$$NiCo_2S_4 + OH^- + H_2O \leftrightarrow NiSOH + 2CoSOH + e^- \quad (2)$$

$$CoSOH + OH^- \leftrightarrow CoSO + H_2O + e^- \quad (3)$$

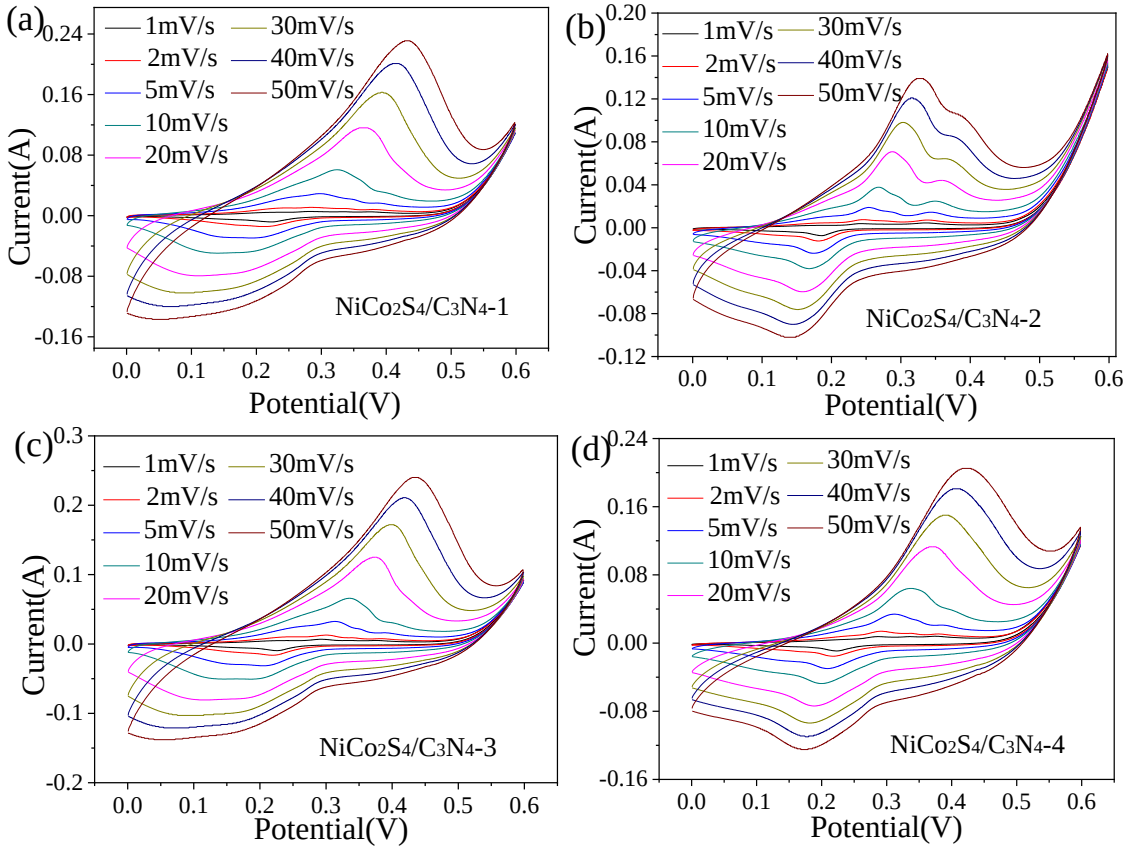

Figure 6. CV curves of (a) $NiCo_2S_4$/g-C_3N_4-1; (b) $NiCo_2S_4$/g-C_3N_4-2; (c) $NiCo_2S_4$/g-C_3N_4-3; and (d) $NiCo_2S_4$/g-C_3N_4-4 composite electrode at different sweep rates.

Fig. 6 (a-d) shows the cyclic voltammograms of the different electrode materials at various scan rates. The integrated area within the loop was increased with the scan rate, similar to the capacitor. In addition, the movement in the oxidation peaks to the right and the reduction peaks to the left was obtained

with an increase in the scan rate. This result may be exemplified by the interfacial polarization of electrolyte ions at higher scan rates.

Table 1. Comparison of different current densities and capacities

Current density	1 A/g (F/g)	2 A/g (F/g)	5 A/g (F/g)	10 A/g (F/g)	15 A/g (F/g)	20 A/g (F/g)	Retention rate
$NiCo_2S_4$/g-C_3N_4-1	1396.7	1327.1	1183.7	1041.6	941.4	882.6	63.19%
$NiCo_2S_4$/g-C_3N_4-2	1175.9	1087.2	997.4	930.8	876.6	834.4	70.96%
$NiCo_2S_4$/g-C_3N_4-3	1406.9	1347.9	1256	1175.5	1115.3	1073.6	76.31%
$NiCo_2S_4$/g-C_3N_4-4	1359.8	1314.9	1229.9	1151	1091.1	1041.8	76.61%
Zhang et al. [39]	(0.5 A/g) 1051	(1 A/g) 973	(2 A/g) 889	(3 A/g) 834	(5 A/g) 678	(8 A/g) 605	57.56%
Liu et al. [40]	(1 A/g) 989.8	(2 A/g) 957.1	(3 A/g) 931.3	(5 A/g) 889.9	(10 A/g) 798.7	(20 A/g) 602.3	60.85%
Vc-$NiCo_2S_4$[41]	(1 A/g) 1046.8	(2 A/g) 984	(3 A/g) 925	(5 A/g) 821	(8 A/g) 696	(10 A/g) 688	65.8%
C_3N_4/PPy/MnO_2[42]	(1 A/g) 509.4	(2 A/g) 426	(3 A/g) 384.1	(5 A/g) 336.3	(10 A/g) 204.3	/	40.1%

Fig.7(a), (b), (c) and (d) shows the charge-discharge curves of samples at various current densities ranging from 1 to 20 A/g. All the curves were symmetric in nature, indicating the high reversibility and rate capability of the electrode. The shape of GCD curve shows a higher degree of similarity with the curve of the pure pseudo-capacitance electrode material, also indicating that the electrode material has an excellent rate performance. However, the shape of the GCD curve of the composite samples is slightly different from that of the pure pseudocapacitive electrode material, which is mainly due to the synergistic effect of the electrode material on its electrochemical performance. The specific capacitance (Cs) of all the electrodes at various current densities was calculated, and the results are shown in Fig.7(e). As observed, the $NiCo_2S_4$/g-C_3N_4-3 electrode had the highest Cs (1406.9 F/g) at 1 A/g, which was decreased to 1073.6 F/g at 20 A/g, retaining a good rate capability of 76.31% with a 20 times enhancement in the current density. On the other hand, the $NiCo_2S_4$/g-C_3N_4-1, $NiCo_2S_4$/g-C_3N_4-2 and $NiCo_2S_4$/g-C_3N_4-4 electrodes had the highest Cs (1396.7 F/g , 1175.9 F/g and 1359.8 F/g, respectively) at 1 A/g, which was decreased to 882.6 F/g , 834.4 F/g and 1041.8 F/g, respectively, at 20 A/g, exhibiting a rate capability of 63.19%, 70.96% and 76.61%, respectively. The enhanced rate capability of the $NiCo_2S_4$/g-C_3N_4-3 electrode may be attributed to the combined effect of the large active surface area, high electronic conductivity, and multiple oxidation states ($Ni^{2+/3+}$, $Co^{2+/3+}$) for charge-storing electrochemical reactions. It is obvious from the above data that with the increase of the composite mole ratio from 0.1:1 to 0.3:1, the electrode material capacity retention rate rapidly increases, but it improves about 0.3% when the composite mole ratio increased from 0.3:1 to 0.4:1, which indicates that the g-C_3N_4 makes a little contribution to electrochemical performance of the electrode material. It

can be seen from Table 1 that the capacitance retention rates of $NiCo_2S_4$ electrode materials prepared by Zhang et al.[39] Liu et al.[40] and Zhang et al.[41] are only 57.56% , 60.85% and 65.8%. It can be seen from this paper that the electrochemical performance of g-C_3N_4 and $NiCo_2S_4$ composites is much higher than that of $NiCo_2S_4$ composites prepared by Yan , Liu and Zhang.

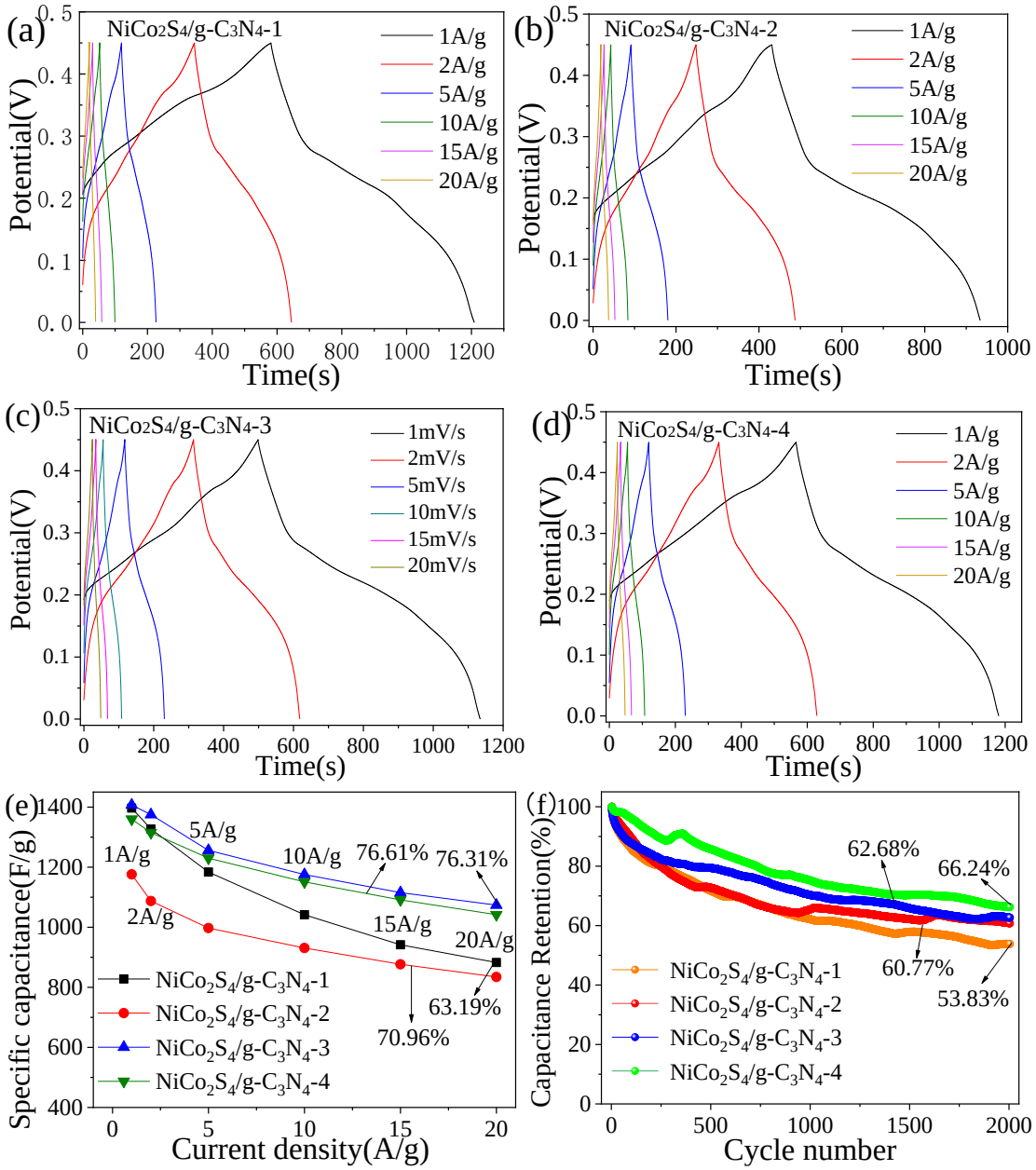

Figure 7. GCD curves of (a) $NiCo_2S_4$/g-C_3N_4-1; (b) $NiCo_2S_4$/g-C_3N_4-2, (c) $NiCo_2S_4$/g-C_3N_4-3; and (d) $NiCo_2S_4$/g-C_3N_4-4 composite electrode at at various current densities; (e) Specific capacitances of different $NiCo_2S_4$/g-C_3N_4 samples at various current densities ranging; (f) Charge–discharge cycling test at the current density of 5 A/g in 5.0 M KOH electrolytes.

The specific capacitance of PPy/MnO_2 prepared by Hamed et al is only 378.4 F/g and the capacity retention rate is 25.6% at 1A/g, but the specific capacitance and capacity retention rate of MnO prepared by Hamed et al.[42] increases to 509.4 F/g and 40% at 1 A/g, respectively. But the specific capacitance

of PPy/MnO_2 prepared by Hamed et al.[42] increases to 509.4 F/g and the capacity retention rate to 40% at 1A/g when the material is compounded with C_3N_4.

Then Fig.7(g) shows the capacitance retention rates of four kinds of electrodes, $NiCo_2S_4$/g-C_3N_4-1, $NiCo_2S_4$/g-C_3N_4-2, $NiCo_2S_4$/g-C_3N_4-3 and $NiCo_2S_4$/g-C_3N_4-4, are 53.83%, 60.77%, 62.68% and 66.24%, respectively, demonstrating that with the increase of the compound ratio of g-C_3N_4, the capacity retention rate is also increasing, which attributes to the synergistic effect of the two materials increases with the increase of the content of g-C_3N_4.

Fig. 8(a-b) are the Nyquist plot of the electrodes observed at zero bias potential in the frequency range of 100 kHz to 100 MHz with an alternating current amplitude of 10 mV. Fig.8(b) is the amplification diagram of impedance plots in Fig.8(a). The intersection point of the EIS curve with the X-axis (y=0) represents the charge transfer resistance, and the resistance values listed in Table 2 are 0.48, 0.466, 0.459 and 0.451 Ω respectively. However, the charge transfer resistances of $NiCo_2S_4$NFs and $NiCo_2S_4$NF prepared by Wu et al.[43] and Chen et al.[44] are 0.61 Ω and 0.58 Ω, respectively [43], and its charge transfer resistance is larger compared to our results.This experimental result further indicates that g-C_3N_4 can reduce the internal resistance of materials.

It can be clearly seen from Fig.8(b) that the charge transfer resistance in the electrode material decreases with the increase of the composite content of g-C_3N_4 in the electrode material, indicating that the charge transfer rate increases with the increase of the composite content of g-C_3N_4 in the electrode material. The low charge transfer resistance (Rct) of the electrode may be attributed to the synergistic effect that enhances the number of surfaceactive sites, promoting charge transfer processes.

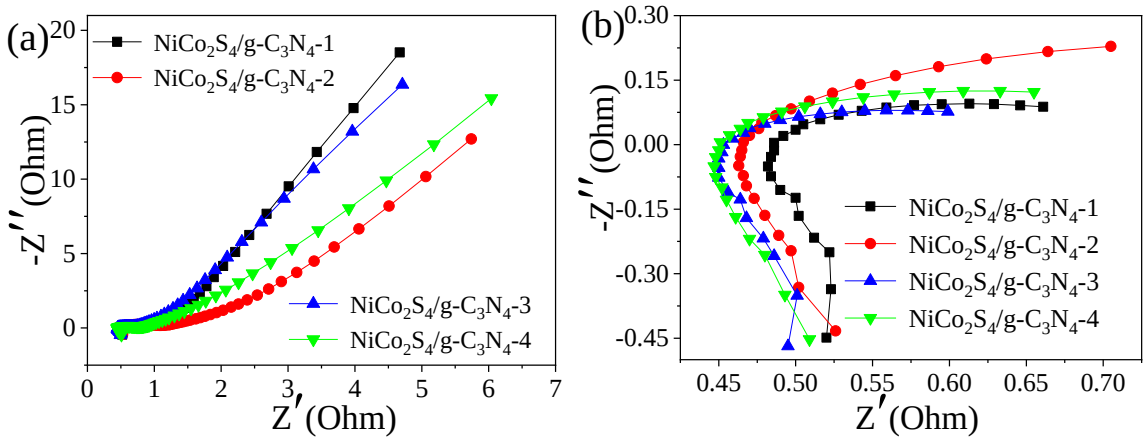

Figure 8. (a-b) Impedance Nyquist plots of different molar ratios $NiCo_2S_4$/g-C_3N_4

Table 2 The point where the curve intersects the X-axis

Material	**Y=0 (Resistance)**
$NiCo_2S_4$/g-C_3N_4-1	0.480 Ω
$NiCo_2S_4$/g-C_3N_4-2	0.466 Ω
$NiCo_2S_4$/g-C_3N_4-3	0.459 Ω
$NiCo_2S_4$/g-C_3N_4-4	0.451 Ω
$NiCo_2S_4$ NSs and $NiCo_2S_4$@$NiCo_2S_4$-2[43]	0.61 Ω and 0.56 Ω
$NiCo_2S_4$/NF [44]	0.58 Ω

4. CONCLUSIONS

In summary, 3D porous $NiCo_2S_4$/g-C_3N_4 have been successfully synthesized. The addition of g-C_3N_4 and the multihole morphology not only shows high conductivity, but also enhances effective channels to improve efficient transport of ions with improved long-termcy stability. With the increase of g-C_3N_4 composite proportion, the capacity retention of electrode material also increases. It is worth noting that the specific capacitance continues to increase with the composite proportion varying from 10% to 40%. These results show that g-C_3N_4 holds great promise in electrochemical applications, and are beneficial for further improvements in the electrodes for electrochemical reactions.

ACKNOWLEDGEMENT
This work was supported by the National Natural Science Foundation of China (No. 12162023 & 51261015), Key R&D Program of Gansu Province-International Cooperation Project (No. 20YF8WA064), and Hong Liu First-Class Disciplines Development Program of Lanzhou University of Technology.

References

1 E. Gökmeşe, *Int. J. Electrochem. Sci.*, 6 (2011) 103.
2 D.H. Deng, H. Pang, J.M. Du, J.W. Deng, S.J. Li, J. Chen and J.S. Zhang, *Cryst. Res. Technol*., 47 (2012) 10.
3 C.J. Yao, Y. Su, Y. Li, J. Li, *Int. J. Electrochem. Sci*., 16 (2021) 150917.
4 K.A. Owusu, L. Qu, J. Li, Z. Wang, K. Zhao, C. Yang, K.M. Hercule, C. Lin, C. Shi and Q. Wei, *Nat. Commun*, 8 (2017) 14264.
5 A. Jain, B.J. Paul, S.J. Kim, V.K. Jain, J. Kim and A.K. Rai, *J. Alloys Compd*., 772 (2019) 72.
6 A. Guo, X. Fang, B. Li, Y. Shi, C. Ouyang, Y.S. Hu, Z. Wang, G.D. Stucky and L. Chen, *Chem. Mater.,* 24 (2012) 457.
7 H.B. Rong, Y.M. Qin, Z.Q. Jiang, Z.J. Jiang and M.L. Liu, *J. Alloys Compd*., 731 (2018) 1095.
8 S.H. Kim, Y.I. Kim, J.H. Park, J.M. Ko, *Int. J. Electrochem. Sci*., 4 (2009) 1489.
9 Y. Yang, Y. Yang, S. Chen and Q. Lu, L. Song, Y. Wei, X. Wang, *Nat. Commun*., 8 (2017) 1559.
10 Y.X. Shi, X.F. Pan, B. Li, M.M. Zhao and H. Pang, *Chem. Eng. J.,* 343 (2018) 427.
11 Y.T. Dong, X.J. Wang, J.L. Chen, F.L. Chai and X.Q. Liu, *Cryst. Res. Technol*., 48 (2013) 8.
12 K.M. Hercule, Q. Wei, A.M. Khan, Y. Zhao, X. Tian and L. Mai, *Nano Lett*., 13 (2013) 5685.
13 N. Wang, H.T. Pang, H.R. Peng, G.C. Li and X.G. Chen, *Cryst. Res. Technol*., 44 (2009) 11.
14 L. Hu, Y. Ren, H. Yang and Q. Xu, *ACS Appl. Mater. Interfaces*, 6 (2014) 14644.
15 K.M. Hercule, Q. Wei, A.M. Khan, Y. Zhao, X. Tian and L. Mai, *NanoLett*., 13 (2013) 5685.
16 H. Zhang, Y. Li, Z. Hong and M. Wei, *Mater. Lett*. 79 (2012) 148.
17 Y.D. Mo, Q. Ru, X. Song, S.J. Hu, L.Y. Guo and X.Q. Chen, *Electrochim. Acta* 176, 575 (2015).
18 X. Han, X. Gui, T.F. Yi, Y. Li and C.B. Yue, *Curr. Opin. Solid State Mater*, 22 (2018) 109.
19 Y.P. Gao, X. Wu, K.J. Huang, L.L. Xing, Y.Y. Zhang and L. Liu, *CrystEngComm*, 19 (2017) 404-418.
20 Y. Wang, P.C. Liu, K.J. Zhu, J. Wang, K. Yan and J.S. Liu, *Electrochim. Acta*, 273 (2018) 109.
21 Y.X. Cui, J. Zhang, C. Jin, Y.X. Liu, W.H. Luo and W.J. Zheng, *Small* 5 (2018) 180431.
22 V. Raman, N.V. Mohan, B.Balakrishnan, R.Rajmohan and H.J. Kim, *Ionics*, 26 (2019) 345.
23 X. Ma, L. Zhang, G.C. Xu, C.Y. Zhang, H.J. Song, Y.T. He, C. Zhang and D.Z. Jia, *Chem. Eng. J.,* 320 (2017) 22.
24 Z. Wang, L. Li, Y. Yu, C. Yang, *Nano*, 15 (2020) 2050052.

25 Y.P. Liu, Z.L. Li, L. Yao, S.M. Chen, P.X. Zhang and L.B. Deng, *Chem. Eng. J*., 366 (2019) 550.
26 Y.W. Zheng, X.X. Wang, W. Zhao, X.W. Cao and J.Q. Liu, *Chem. Eng. J*., 333 (2018) 603.
27 G.H. Yu, X. Xie, L.J. Pan, Z.A. Bao and Y. Cui, *Nano. Energy*, 2 (2013) 213.
28 H.F. Jiu, L.Y. Jiang, Y.Y. Gao, Q. Zhang and L.X. Zhang, *Ionics,* 25 (2019) 4325.
29 X.L. Zhu, Z.Q. Wei, L. Ma, J.H. Liang and X.D. Zhang, *B. Mater. Sci*., 43 (2020) 1.
30 L. Yu, L. Zhang, H.B. Wu and X.W.D. Lou, *Angew. Chem. Int. Ed.*, 53 (2014) 3711-3714
31 X.R. Han, C. Qun, H. Zhang, Y.H. Ni and L. Zhang, *Chem. Eng. J*., 368 (2019) 513-524.
32 H. He, G. Wang, B. Shen, Y. Wang and Z. Xiao, *J. Solid. State. Chem*., 288 (2020) 121375.
33 S. Dai, B. Zhao, C. Qu and D.C. Chen, *Nano Energy*, 33 (2017) 522.
34 W. Xia, C. Qu, Z. Liang, B. Zhao, S. Dai, B. Qiu, Y. Jiao, Q. Zhang, X. Huang and W. Guo, *Nano Letters*, 27 (2017) 88.
35 M.D. Lan, F. Wang, Y.Y. Wu, W. Li, Y. Qiu, L.X. Fang and Q.S. Jing, *J. Mater. Sci. Mater. Electron.*, 29 (2018) 21109-21118.
36 X.W. Chang, W.L. Li, Y.H. Liu, M. He, X.L. Zheng, J.B. Bai and Z.Y. Ren, *j. colloid interface sci.*, 538 (2019) 34-44.
37 M. Govindasamy, S. Shanthi , E. Elaiyappillai, S.F. Wang, P. M. Johnson, H. Ikeda, Y. Hayakawa, Su. Ponnusamy and C. Muthamizhchelvan, *Electrochimica Acta*, 293 (2019) 328-337.
38 S.H. Zhao, Z.B. Yang, W.W. Xu, Q.Y. Zhang, X.M. Zhao, and X. Wen, *Electrochimica Acta*, 297 (2019) 334-343.
39 Y. Zhang, X.Z. Wang, M. Shen, X. Fu, M. Huang, X.Y. Liu, and Y. X. Zhang, J Mater Sci., 54 (2019) 4821-4830.
40 Y.P. Liu, Z.L. Li, L. Yao, S.M. Chen, P.X. Zhang, and L.B. Deng, *Chemical Engineering Journal*, 366 (2019) 550-559.
41 Y. Zhang, L. Ye, J.H. Guo, Y. Y. Shang, F. M.i Guo, Y. J. Zhang, and J. Xu, *J Mater Sci.*, 56 (2021) 9368-9381.
42 P. Hamed, B. Ramin, G. Mostafa, M. Saremi, H. Pourfarzad, R. Badrnezhad, M. Ghaemmaghami, *Ionics*, 27 (2021) 4057-4067.
43 W. L. Wu, C. H. Zhao, C. W. Wang, T. T. Liu, L. Wang, J. F. Zhu, *Applied Surface Science*, 563 (2021) 150324.
44 H. Q. Chen, J. Xiang, R. D. Zhao, Y. Guo, S. Loy, F. F. Wu, S. H. Chen, *Ionics*, 27 (2021) 867-874.

© 2022 The Authors. Published by ESG (www.electrochemsci.org). This article is an open access article distributed under the terms and conditions of the Creative Commons Attribution license (http://creativecommons.org/licenses/by/4.0/).